AN EXPERIMENTAL INVESTIGATION OF FLOW-INDUCED NOISE MECHANISM OF A FLEXIBLE FLAT-PLATE TRAILING-EDGE

Chandrashnata Das[1], Akhilesh Mimani[1], Ric Yang Porteous[1], Con J. Doolan[2]

[1]School of Mechanical Engineering
University of Adelaide, Adelaide SA 5005, Australia
Email: chandrashnata.das@student.adelaide.edu.au
akhilesh.mimani@adelaide.edu.au
ric.porteous@adelaide.edu.au

[2]School of Mechanical and Manufacturing Engineering
UNSW Australia, Sydney NSW 2052, Australia
Email: c.doolan@unsw.edu.au

Abstract

The Trailing-Edge (TE) of aircraft wings generates significant noise which is problematic for communities. This paper investigates a possible noise reduction mechanism by using an airfoil with a flexible TE made from Nylon 6 material. Experiments were carried out in an Anechoic Wind Tunnel (AWT) at low-to-moderate Reynolds number $2.8 \times 10^5 < Re < 4.3 \times 10^5$, based on the chord length. To this end, two different flexible TE models with different chord-wise lengths are studied and their results are compared with that obtained for the rigid TE models (made of aluminium) at different free-stream velocities. A spiral array comprising of 31 microphones were used to record the acoustic pressure data for the different test-cases during aeroacoustics experiment. The Power Spectral Density (PSD) spectra obtained from single microphone measurements indicate a noise reduction of 4 dB (on average) whilst using a flexible TE in comparison to its rigid counterpart, thereby demonstrating the effectiveness of a flexible TE for reducing noise. Cross-spectral Conventional Beamforming (CB) was implemented using the recorded acoustic pressure for the TE models considered to obtain a source map. The source maps indicate a dominant TE noise source at high-frequencies (i.e., in the one-third octave bands with centre frequencies 3150 Hz onwards) whilst a dominant Leading-Edge (LE) noise source is observed in the one-third octave bands whose centre frequencies are 2000 Hz and 2500 Hz (the mid-frequency range) which is in agreement with the results of previous investigations.

1. Introduction

The flow-induced noise generated by the Trailing-Edge (TE) of an airfoil is one of the major airframe noise contributors that is dominant during take-off and landing of aircraft. Previous studies have focused on developing numerical and experimental models to understand the TE noise [1-3]. For example, Brooks *et al.* [4] discuss the major factors responsible for noise generation at the TE of an airfoil. Large Eddy Simulation (LES) on a NACA0012 airfoil were conducted with tripped boundary-layers and blunt rounded TE for three different flow configurations for a Reynolds number (Re_c) equal to 4.08×10^5 (depending on the chord-length of the flat-plate). Based on these results, it was noted that there exist a variety of airfoil self-noise mechanisms, namely, (1) TE bluntness vortex-shedding, (2) interaction of the airflow turbulence with the edge, (3) flow separation occurring near the TE area (separation-stall TE noise), and (4) scattering of velocity fluctuations. Early theoretical work on TE

noise was carried out by Lighthill [5] as well as Ffowcs Williams and Hall [6]. Other papers include a review of different theories of sound generation at the TE of a semi-infinite rigid-plate, see Howe [7], the theory of noise prediction using measured surface pressures by Brooks *et al.* [8], detailed self-empiric relations for airfoil self-noise due to pressures by Brooks *et al.* [9] and empirical models for prediction by Schinkler *et al.* [10].

Of particular research interest are wings of an owl that is well-known for its silent flight. This is possible due to three distinctive features of its wing, namely, the poroelastic filaments at the TE of the feather and wings, (2) the stiff feathers at the Leading-Edge (LE) of the wing, and (3) the soft downy coating on the upper surface [11], [12]. On careful consideration of these features, various ideas have been adopted with a view to reduce airfoil noise, some of them include the use of a serrated TE [7, 13, 14], porous airfoil and elastic TE [1], use of a modified NACA 63-215 airfoil model with different TE bluntness by Brooks and Hutcheson [15], use of a flexible polypropylene TE brush model at the airfoil TE section proposed by Herr [2] and Finez *et al.* [16]. In particular, Finez *et al.* [16] studied the noise suppression mechanism obtained by the use of a brush formed of a single row of flexible polypropylene fibers at the TE section of a NACA profile at Reynolds number (Re_c) ranging from 1.73 x 10^5 to 3.47 x 10^5 (based on chord-wise length of the airfoil). The Power Spectral Density (PSD) obtained from the experiments exhibit a noise reduction of 3 dB in the frequency range 600 Hz to 2000 Hz. Furthermore, it was noted that due to the generation of noise source generated at the vicinity of the LE section, the overall noise reduction was affected. Therefore, it was concluded that the flexible TE brushes can efficiently reduce broadband noise generated at the TE in the low-frequency range; however, in the mid-frequency range of 2000 Hz to 4000 Hz, LE noise dominated the results.

The aforementioned features certainly reduce the airfoil TE noise; however, the noise reduction capability of a flexible (or compliant) TE flat-plate has not yet been experimentally demonstrated. The present work therefore, demonstrates the TE noise reduction mechanism of a flexible TE flat-plate through aeroacoustics experiments in a wind tunnel. An approach similar to that adopted by Herr *et al.* [2] and Finez *et al.* [16] is used here wherein the TE configurations of flat-plate is altered using a flexible polypropylene brush (made of Nylon 6 material). The scope of this work is limited to studying the turbulent boundary-layer and vortex-shedding noise at the flat-plate TE section. The present investigation is carried out by considering a turbulent flow over the test-cases (flat-plate with different TE configurations) and these test-cases are mounted at zero angle of attack to minimise stall phenomenon.

This paper is organised as follows. Section 2 discusses the experimental set-up and the data processing techniques used. Section 3 presents the experimental results which include the PSD spectra of the far-field radiated noise, the source maps obtained using Conventional Beamforming (CB) and the spatial integration plots. The paper is concluded in Section 4.

2. Experimental investigation

2.1 Anechoic Wind Tunnel

The aeroacoustics experiments were conducted in the Anechoic Wind Tunnel (AWT) of the University of Adelaide. The internal dimensions of the AWT are 1.4m x 1.4 m x 1.6 m and its main components are the contraction-outlet, settling chamber, silencer and fan in an acoustic enclosure, collector and diffuser. The rectangular contraction-outlet has a width w = 275 mm and a height h = 75 mm [14, 17]. The walls of the AWT are treated acoustically with foam wedges attached to its walls to provide a reflection-free environment for frequencies greater than 250 Hz. The maximum free stream velocity in the AWT is $40\ \mathrm{m\cdot s^{-1}}$ whilst the free-stream turbulence intensity is 0.33 % [14, 17]. In this work, experiments were conducted for three different mean flow velocities given by $U_\infty = \{25,\ 30,\ 35\}\ \mathrm{m\cdot s^{-1}}$ and a spiral array comprising of 31 microphones (located at the top along the ceiling of the AWT) were used to record the far-field radiated acoustic pressure data for different test-cases. The microphones were calibrated post-installation to take into account the airflow noise.

2.2 Flat-plate and the TE plate design

A flat-plate was used as the test-model and the designed flexible (compliant) edges were attached at the TE of the flat-plate. This plate has a span-wise length of 450 mm, chord-wise length of 150 mm without a TE plate and a thickness of 5 mm. The LE of the plate is elliptical in shape with a semi-minor axis of 3 mm and a semi-major axis of 8 mm and the TE section is wedge-shaped with angle of 12° [14]. Figure 1 shows the schematic diagram of the flat-plate.

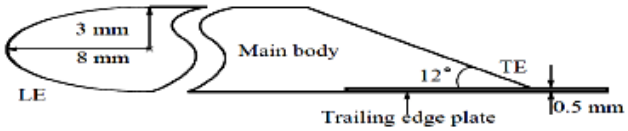

Figure 1. Flat-plate design used by Moreau *et al.* [14].

In order to mount the flexible TE plate on the main body (shown in Fig. 1), a holder plate (shown in Fig. 2(a)) was used. This holder plate and the TE configurations used during the tests were fabricated depending on the dimensions and specifications of the flat-plate as given in Moreau *et al.* [14]. The two overall chordwise lengths considered during in this work when the flat-plate was mounted with the different TE plate designs were 168 mm and 183 mm and the chord-wise lengths of the TE plate models were 90 mm and 105 mm, respectively. Figure 2(a) presents a schematic of the holder plate and the TE plate that were mounted at the flat-plate TE section whilst a photograph depicting the flat-plate model with a compliant TE attached to the contraction-outlet of AWT is presented in Fig. 2(b).

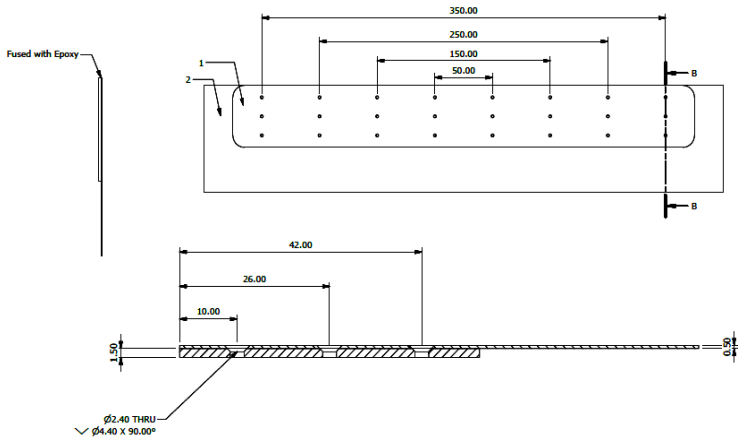

(a)

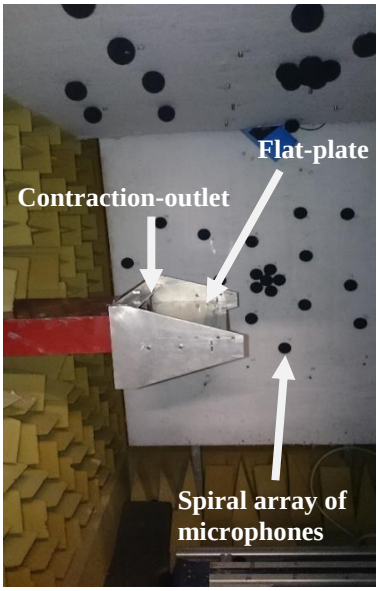

(b)

Figure 2. (a)TE plate attached with the holder plate (Plate 1 is the holder plate and plate 2 is the TE plate). (b) Flat-plate model with a compliant TE attached to the contraction-outlet of AWT.

In order to vary the TE flexibility of the considered flat-plate, four different TE plate designs with different flexural rigidity were fabricated. The material selected for fabricating the different TE designs are specified in Table 1.

It is noted that Herr *et al.* [2] as well as Finez *et al.* [16] used polypropylene material to fabricate the TE configuration due to its high-strength and rigidity and its resistance to corrosion as well as other physical damages. However, in the current study Nylon 6 is selected for fabricating the flexible TE plates in place of polypropylene polymer, which also has a high-strength. The experimental data set obtained for the flexible edged flat-plate was compared to the data obtained for the rigid edged flat-plate made of Aluminium alloy.

Table 1. Different TE plate designs

Test-case	Description	Material	Chord-wise length (mm)	Elastic Modulus (GPa)	Flexural rigidity $\left(\mathrm{Pa}\cdot\mathrm{m}^4\right)$
1	Rigid plate	Aluminium alloy	90	73	2×10^6
2	Rigid plate	Aluminium alloy	105	73	3.2×10^6
3	Flexible plate	Nylon 6	90	3	8.2×10^4
4	Flexible plate	Nylon 6	105	3	1.3×10^5

2.3 Data Processing

The far-field acoustic pressure was recorded over a spiral array comprising of 31 GRAS precision microphones connected to National Instruments PXI-8016 data acquisition system containing 4 PXI-4496 simultaneous sample and hold ADC cards. Microphone data was recorded at a sampling frequency $f_s = 2^{16}$ Hz for a sampling time of 40 s and presented in one-third octave band and narrow band format with a frequency resolution of 64 Hz. A Power Spectral Density (PSD) versus frequency plot was generated using Welch's function with a Hanning window of length 65536 samples each, and a 50% overlap. Simultaneously, a cross-spectral matrix was calculated using Conventional Beamforming (CB). Spatial integration of the noise level over the LE and TE is carried out to quantify the individual contribution of noise generated by each region of interest (i.e., by the TE and Leading-Edge (LE)) over the flat-plate. To this end, the $3/8^{\text{th}}$ Simpson's integration rule [18] was used over two rectangular areas containing the LE and TE sections. The side-lobes at the corners of the flat-plate as shown in the CB maps are not considered because they are representative of end-effects, i.e., they are generated due to interaction of the flow with the test-rig on the sides to which the flat-plate is attached and tends to cause an error in the interpretation of spatial-integration results.

3. Experimental results and discussion

3.1 Acoustic Data

The far-field acoustic spectra of the flat-plate with a rigid reference TE plate and a flexible TE plate of 90 mm dimension at free-stream velocity of $U_\infty = 35\ \mathrm{m}\cdot\mathrm{s}^{-1}$ and $\mathrm{Re} = 3.9\times10^5$ is shown in Figure 4. The background noise is also shown in the PSD graph. From Fig. 4, it is evident that the broadband noise decreases in case of the flexible TE flat-plate as compared to its rigid counterpart. This decrease in level is observed in the low-frequencies range less than 3.3 kHz (where the corresponding Strouhal number St_t = 0.048). A peak is observed in the noise spectra towards the high-frequency range above 8.9 kHz. These high frequency peaks are a result of vortex-shedding noise from the TE [14] and as observed from Fig. 4, attenuation in the peak level is obtained when the flexible TE plate is used instead of the rigid TE plate with the flat-plate. The centre frequencies f_c of the sharp peaks in the PSD spectra with the associated Strouhal number (normalised by the TE thickness i.e. 0.5 mm) for each test cases is specified in Table 2. It is noted that the Strouhal number $St_t = f_v t/U_\infty$ where f_v is the vortex shedding frequency, t is the thickness of the flat-plate and U_∞ is the free-stream velocity.

Table 2. Vortex shedding frequency f_v and Strouhal Number St_t of TE vortex shedding noise generation at a flow speed of $U_\infty = 35\ \mathrm{m\cdot s^{-1}}$.

Free-stream velocity U_∞ = 35 m·s^{-1}	Vortex shedding frequency f_v (in Hz)	Strouhal Number (St_t)
Flexible TE (90mm)	8988	0.1284
Flexible TE (105mm)	8253, 8428 and 9338	0.1179, 0.1204 and 0.1334
Reference TE (90mm)	9009	0.1287
Reference TE (105mm)	8393 and 9296	0.1199 and 0.1328

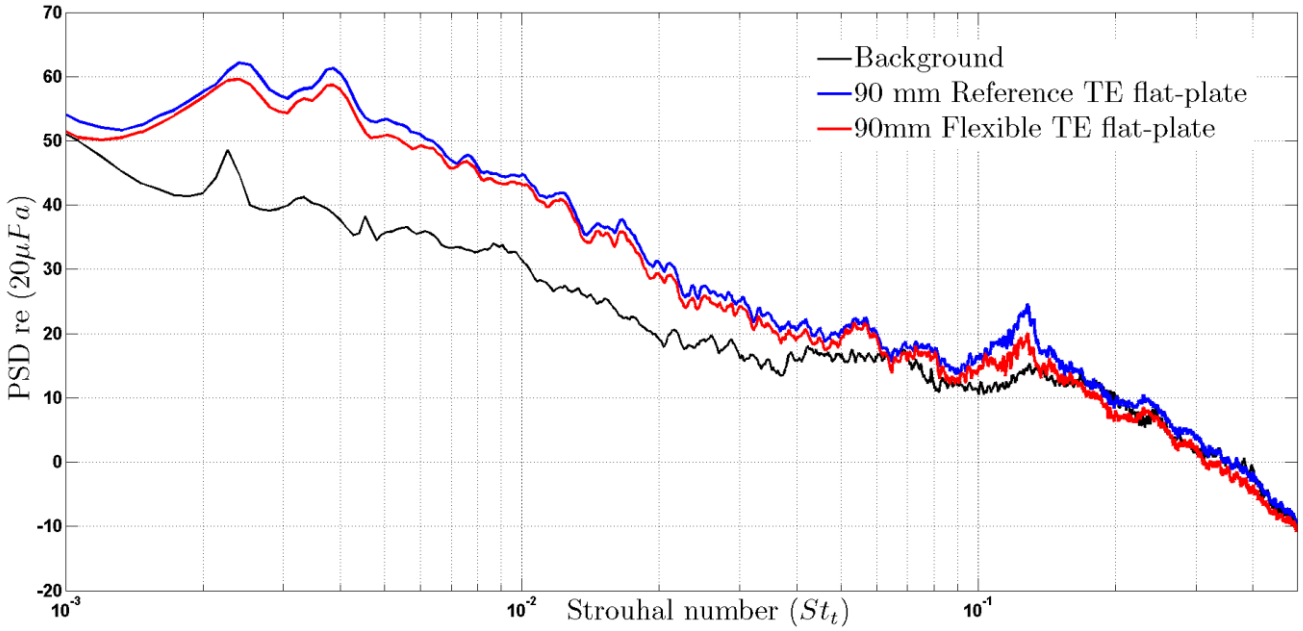

Figure 4. PSD of the flat-plate with rigid reference TE and flexible TE at a free-stream velocity $U_\infty = 35\ \mathrm{m\cdot s^{-1}}$ (both the TE plates are of 90 mm chord-wise length).

Additionally, other experiments were conducted to record the acoustic noise spectra for the four test cases at different flow velocities of 25 m/s and 30 m/s. However, in this paper, the results obtained at mean flow $U_\infty = 35\ \mathrm{m\cdot s^{-1}}$ is presented due to brevity. Nonetheless, similar results were also obtained for lower flow speeds. It is noted that Finez *et al.* [16] demonstrated significant noise attenuation in the low-frequency range around 1000 Hz when a flexible polypropylene brush fibre was used at the TE section of NACA65 (12)-10 airfoil. The results from the current study are in a close agreement to that obtained by Finez *et al.* [16]. Furthermore, Finez *et al.* [16] note that the noise reduction for the particular configuration are higher than observed from PSD results because the attenuation was limited by the LE noise source emission in the frequency range between 2 kHz to 4 kHz. The present investigation is shown to be consistent with Finez *et al.* [16] because the LE noise sources are observed within the frequency range of 2 kHz to 3.15 kHz. A detailed study of noise source emission and sound intensity levels for the flexible and rigid TE flat-plate are discussed in the ensuing section.

3.2 Conventional Beamforming (CB)

The parts (a) of Figs. 5 to 10 show the source maps that indicate the different sound sources generated by the flexible TE flat-plate while part (b) of the corresponding figures show the sources generated by the rigid TE flat-plate for a flow speed of $U_\infty = 35\ \mathrm{m\cdot s^{-1}}$ for six different one-third octave band frequencies. (It is noted that the colorbar in these source maps indicate the intensity of the noise sources.) A noticeable difference in the intensity of the noise sources and its locations over the flat-plate is observed when the plate with flexible TE is compared with its rigid counterpart. Within the frequency range of 2000 Hz to 2500 Hz, the LE noise sources are observed (It is noted that the CB source map at 2000 Hz is not shown here). This is consistent with the study by Finez *et al.* [16] where

a strong emission of LE noise sources were encountered between the frequencies ranges of 2000 Hz to 4000 Hz. However, slight differences in the set of results obtained in the present study might be due to the difference in the model designs used and other external factors.

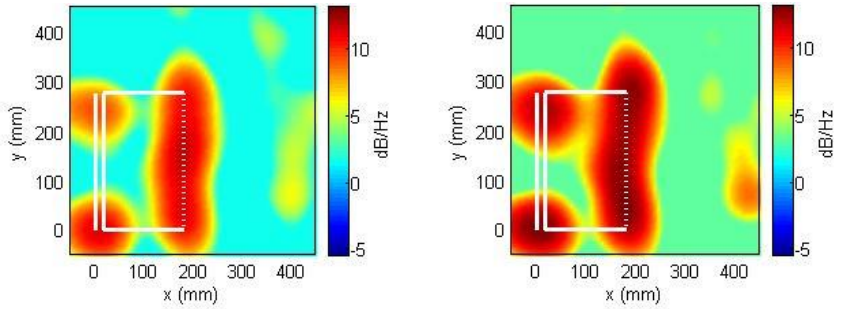

a. Flexible TE plate (90 mm) b. Reference TE plate (90 mm)

Figure 5. CB source maps of the flexible and reference TE flat-plates having 90 mm TE plates (chord-wise) at a flow speed of $U_\infty = 35\ \mathrm{m \cdot s^{-1}}$ (at centre band frequency f_c = 2500Hz)

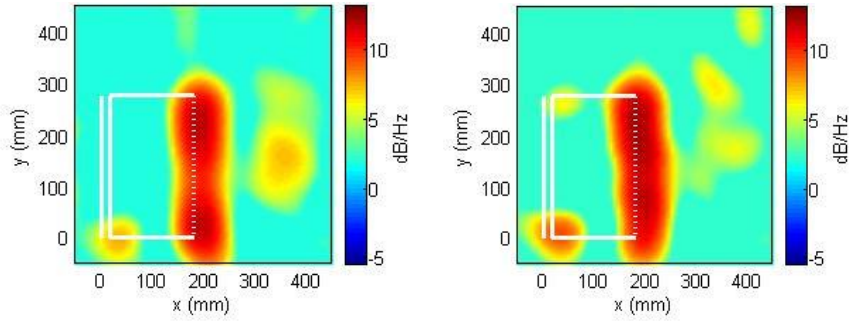

a. Flexible TE plate (90 mm) b. Reference TE plate (90 mm)

Figure 6. CB source maps of the flexible and reference TE flat-plates having 90 mm TE plates (chord-wise) at a flow speed of $U_\infty = 35\ \mathrm{m \cdot s^{-1}}$ (at centre band frequency f_c = 3150Hz)

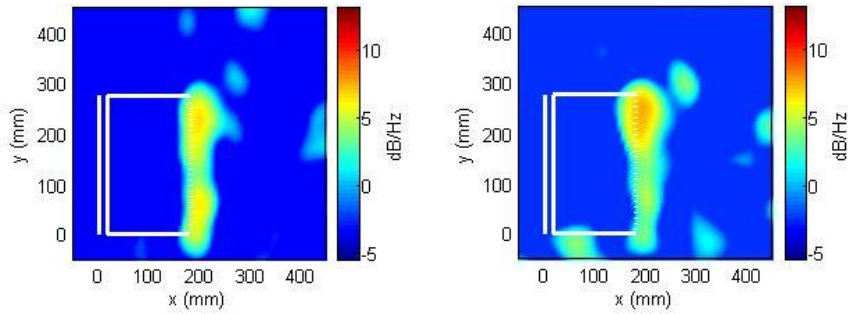

a. Flexible TE plate (90 mm) b. Reference TE plate (90 mm)

Figure 7. CB source maps of the flexible and reference TE flat-plates with 90 mm TE plates (chord-wise) at a flow speed of $U_\infty = 35\ \mathrm{m \cdot s^{-1}}$ (at centre band frequency f_c = 4000Hz).

It is observed from Figs. 5(a) and (b) that in the frequency range below 3150 Hz, two noise source locations exist, one at the TE section and the other at the LE section of the flat-plate. These noise sources are associated with the turbulent boundary-layer TE noise, turbulence-interaction noise and possibly small recirculation bubble near the LE, respectively [16]. Dominant TE noise sources are observed at higher frequencies of the one-third octave bands, i.e. frequencies beyond 3150 Hz as also observed in Mimani *et al*. [17] for the symmetric flat-plate test-case.

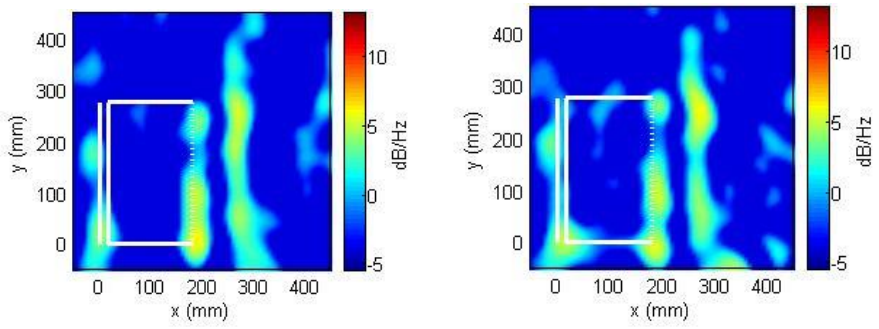

a. Flexible TE plate (90 mm) b. Reference TE plate (90 mm)

Figure 8. CB source maps of the flexible and reference TE flat-plates having 90 mm TE plates (chord-wise) at a flow speed of $U_\infty = 35\ \mathrm{m \cdot s^{-1}}$ (at centre band frequency f_c = 5000Hz).

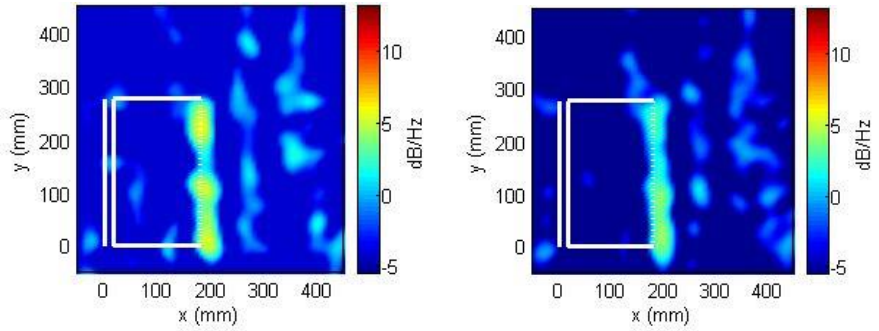

a. Flexible TE plate (90 mm) b. Reference TE plate (90 mm)

Figure 9. CB source maps of the flexible and reference TE flat-plates with 90 mm TE plates (chord-wise) at a flow speed of $U_\infty = 35\ \mathrm{m \cdot s^{-1}}$ (at centre band frequency f_c = 6300Hz)

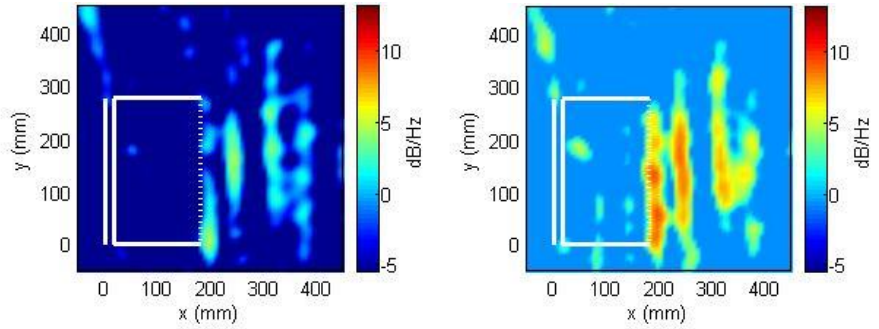

a. Flexible TE plate (90 mm) b. Reference TE plate (90 mm)

Figure 10. CB source maps of the flexible and reference TE flat-plates with 90 mm TE plates (chord-wise) at a flow speed of $U_\infty = 35\ \mathrm{m \cdot s^{-1}}$ (at centre band frequency f_c = 8000Hz)

Figures 5 and 6 show a significant decrease in the intensity of the noise sources at both TE and LE sections when the flexible TE plate is used in comparison to the use of its rigid counterpart. This may be due to the result of TE flexibility which is affecting the aerodynamics of the LE, thereby giving certain noise attenuation at the LE section. However, the physical mechanism behind the noise reduction at the LE section will be investigated in future work. Moving on to a higher frequency range around 4000 to 6300 Hz, the CB source maps (Figures 7 to 9) show a certain amount of increase in the noise source intensity at the vicinity of the TE when the flexible TE flat-plate is compared to the rigid TE flat-plate and in Figure 10, it shows a decrease in the noise source intensity again, in case of the flexible TE flat-plate. From this, it is understood that at a mid-frequency range between 4000 to 6300 Hz, there is a minimal amount of increase in TE noise generation by the flexible TE flat-plate. However, the phenomenon behind it has to be analysed further. The side lobes occurring in the CB

source maps at higher frequency bands are errors due to the influence of point spread function. A similar set of results have also been obtained for the test-cases with 105 mm TE plates at a flow speed of $U_\infty = 35\ \mathrm{m \cdot s^{-1}}$.

The CB source maps at various one-third octave band frequencies obtained for the other test cases at different flow speeds of $25\ \mathrm{m \cdot s^{-1}}$ and $30\ \mathrm{m \cdot s^{-1}}$ also show generation of LE noise sources at the frequency range between 2000 Hz to 3150 Hz. For frequencies above 2500 Hz, the TE section of the flat-plate generates dominant noise sources, similarly like the CB source maps presented above.

3.3 Spatial Integration

Figures 11(a) and (b) show the PSD graph of noise generated from specific regions (LE and TE) of the flat-plate at a flow speed of $U_\infty = 35\ \mathrm{m \cdot s^{-1}}$. Figure 11(a) presents the results of a flat-plate having 90 mm TE plate chordwise length whilst Fig. 11(b) presents the flat-plate results with TE plates of 105 mm chord-wise length. As noted from these graphs, the TE noise is dominant over various range of frequencies compared with the LE noise generation. Thus, it can be stated that the TE noise emission is dominant over the LE noise emission, especially in the high-frequency range [17]. Furthermore, in Fig. 11(a) the attenuation in noise spectra at the TE is significant at higher frequency levels ranging from 5.95 kHz-8.743 kHz where the corresponding Strouhal number range from 0.085-0.125 when flexible TE plate was used instead of the rigid counterpart. Here, a noise reduction of 4 dB (on average) has been obtained within the stated range of frequency. On the other hand, a significant decrease in the noise spectra was noted at the LE section of the flexible TE flat-plate within the high frequency bands when compared to LE section of the rigid TE flat-plate. However, the attenuation in the lower frequencies was negligible. An average of 2-3 dB is observed in the frequency range above 6.3 kHz for the LE section where the corresponding Strouhal number is approximately 0.09-0.12.

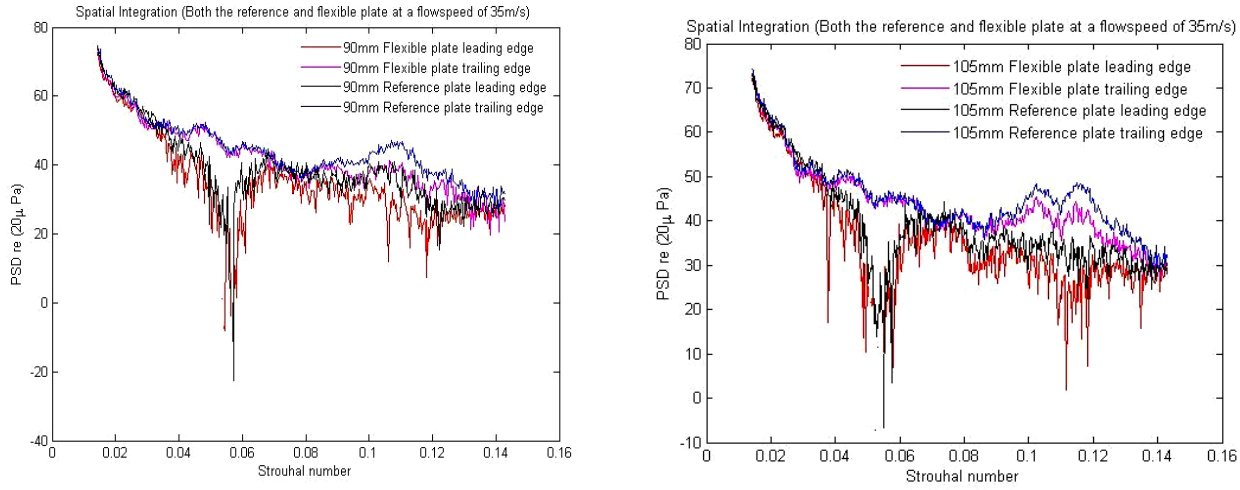

(a) (b)

Figure 11. PSD spectra for the specific region around the LE and TE of the flat-plate with flexible and rigid TE plate designs at a free stream velocity $U_\infty = 35\ \mathrm{m \cdot s^{-1}}$.

Figure 11(b) shows the noise attenuation at the LE section above St_t = 0.1 when the flexible TE plate design of 105 mm chordwise length was used with the flat-plate as opposed to the rigid TE plate of same chordwise length. On the other hand, a decrease in the noise level of approximately 3-4 dB is observed at the TE section within 0.09 - 0.135 Strouhal number. A small noise attenuation was also achieved at the LE section of the flat-plate within Strouhal number range equal to $0.1-0.12$.

From the above results, it is evident that there is both TE and LE noise attenuation, when a flexible TE is used. Also a distinct phenomenon is observed from the presented results at a range of frequency corresponding to Strouhal number, $0.025 < S_t < 0.038$ (approximately) for both the cases presented. Within this specified Strouhal number range, the LE generates dominant noise sources over

the TE noise generation. Furthermore, TE noise attenuation approximately equal to 4 dB was achieved at higher frequency range.

On revisiting the PSD graphs shown in Fig. 4, it is observed that the TE vortex-shedding noise was evident at a Strouhal number of 0.1 (approximately) for all the test-cases. This implies that the noise attenuation encountered in the TE section of the flat-plate in Figs. 11(a) and (b) is the reduction of the vortex-shedding noise due to the effect of flexible TE configuration on flow-induced noise around the flat-plate TE. Also, it is noted that for all test-cases, the TE noise generated is the dominant noise source, especially in the high-frequency range [17] as compared to the LE noise generated.

4. Conclusion

This paper has experimentally investigated the effect of introducing a flexible/complaint Trailing-Edge (TE) at the TE section of a flat-plate on TE noise suppression mechanism at a low-to-moderate range of Reynolds numbers given by $2.8 \times 10^5 < \mathrm{Re}_c < 4.3 \times 10^5$. The aeroacoustics experiments were carried out on the flat-plate model used earlier by Moreau *et al.* [14] which was mounted with different flexible TE plate designs with varying chordwise lengths in an Anechoic Wind Tunnel (AWT).

From the Power Spectral Density (PSD) versus Strouhal number (normalized by the thickness of the TE plates) data, a noticeable trend of noise attenuation by the flexible TE flat-plate over the rigid TE flat-plate was evident, and however, the reduction was minimal. In the lower-frequency range, the reduction in the broadband noise noted may be due to a change in the pressure fluctuation at the TE section by the TE flexibility [19]. During this study, an overall reduction of 2 dB was attained when the flat-plate (with 183 mm chordwise length) was tested at a flow speed of $U_\infty = 35\ \mathrm{m \cdot s^{-1}}$. Furthermore, the Conventional Beamforming (CB) results were obtained to understand the noise source locations. These results show that a dominant Leading-Edge (LE) noise source is observed in the one-third octave bands whose center frequencies are between 2000 Hz and 2500 Hz (the mid-frequency range). The possible justification underlying the noise source generation at the vicinity of the LE and TE of the test-cases within that specified range of frequencies has been investigated and noted earlier. A spatial integration of the PSD spectra was performed in order to quantify the individual contribution of the LE and TE to noise generation of the flat-plate and these results proved that an attenuation in the noise spectra of 4 dB (on an average) was achieved by the flexible edge at the TE area of the flat-plate, at comparatively higher frequencies. In the lower frequencies below 5.95 kHz, the TE areas for both the test-cases with flexible and rigid TE plates show a similar result. In the LE section, a decrease in noise of around 2 - 3 dB (on an average) was noted when the flexible TE was used. However, the noise attenuation mechanism occurring at the LE section of the flat-plate due to the change in the TE plate design is a subject of future investigation.

Acknowledgements

The first author acknowledges the support of the School of Mechanical Engineering, The University of Adelaide.

References

[1] Jaworski, J. W. and Peake, N., "Aerodynamic noise from a poroelastic edge with implications for the silent flight of owls", *Journal of Fluid Mechanics*, **723**, 456–479, (2013).

[2] Herr, M. "Design criteria for low-noise trailing edges", *Proceedings of the 13th AIAA/CEAS Aeroacoustics Conference*, Rome, Italy, 21-23 May 2007.

[3] Geyer, T., Sarradj, E. and Fritzsche, C., "Measurement of the noise generation at the trailing edge of porous airfoils", *Experiments in Fluids*, **48**, 291–308, (2010).

[4] Brooks, T. F., Pope, D. S. and Marcolini, M. A. *Airfoil self-noise and prediction*, NASA Reference Publication 1218, 1989.

[5] Lighthill, M.J. "On sound generated aerodynamically – Part I. General theory", *Proceedings of the Royal Society of London*, **212**, 1-32, (1952).

[6] Ffowcs Williams, J.E. and Hall, L.H. "Aerodynamic sound generation by turbulent flow in the vicinity of a scattering half plane", *Journal of Fluid Mechanics*, **40**, 657-670, (1970).

[7] Howe M. S. "A Review of the theory of trailing edge noise", *Journal of Sound and Vibration*, **61**, 437-465, (1978).

[8] Brooks, T.F. and Hodgson, T.H. "Trailing edge noise prediction from measured surface pressures", *Journal of Sound and Vibration*, **78**, 68-117, (1981).

[9] Brooks, T.F., Pope, D.S. and Marcolini, M.A., "Airfoil self-noise and prediction", *NASA Reference Publication, NASA-RP-1219*, 1989.

[10] Schinkler, R.H. and Amiet, R.K., "Helicopter rotor trailing edge noise", *NASA Contractor Report*, NASA-CR-3470, 1981.

[11] Bachmann, T., Wagner, H. and Tropea, C. "Inner vane fringes of barn owl feathers reconsidered: morphometric data and functional aspects", *Journal of Anatomy*, **221**, 1–8 (2012).

[12] Lilley, G. M. "A study of the silent flight of the owl", *Proceedings of the 4th AIAA/CEAS Aeroacoustics Conference*, Toulouse, France, 2-4 June 1998.

[13] Howe M. S. "Aerodynamic noise of a serrated trailing edge", *Journal of Fluids and Structures*, **5**, 33-45, (1991).

[14] Moreau, D. J. and Doolan, C. J., "Noise-reduction mechanism of a flat-plate serrated trailing edge", *AIAA Journal*, **51**, 2513-2522, (2013).

[15] Brooks, T. F. and Hutcheson, F. V., "Effects of angle of attack and velocity on trailing edge noise", *Proceedings of the 42nd AIA Aerospace Sciences Meeting*, Reno, USA, 5-8 January 2004.

[16] Finez, A., Jondeau, E., Roger, M. and Jacob, M. C., "Broadband noise reduction with trailing", *Proceedings of the 16th AIAA/CEAS Aeroacoustics Conference*, Stockholm, Sweden, 8-9 June 2010.

[17] Mimani, A., Moreau D. J. and Doolan, C. J., "Experimental application of aeroacoustic time-reversal", *Proceedings of the 21st AIAA/CEAS Aeroacoustics Conference*, Dallas, USA, 22-26 June 2015.

[18] Atkinson, K.E. *An introduction to numerical analysis*, 2nd edition, Wiley, Singapore, 2004.

[19] Schalanderer, S. and Sandberg, R. D., "DNS of a compliant trailing edge flow", *Proceedings of the 19th AIAA/CEAS Aeroacoustics Conference*, Berlin, Germany, 27-29 May 2013.